J Intell Robot Syst (2014) 73:429–453
DOI 10.1007/s10846-013-9915-6

Fractional-Order Complementary Filters for Small Unmanned Aerial System Navigation

Calvin Coopmans · Austin M. Jensen · YangQuan Chen

Received: 1 September 2013 / Accepted: 12 September 2013 / Published online: 24 October 2013

Abstract Orientation estimation is very important for development of unmanned aerial systems (UASs), and is performed by combining data from several sources and sensors. Kalman filters are widely used for this task, however they typically assume linearity and Gaussian noise statistics. While these assumptions work well for high-quality, high-cost sensors, it does not work as well for low-cost, low-quality sensors. For low-cost sensors, complementary filters can be used since no assumptions are made with regards to linearity and noise statistics. In this article, the history and basics of complementary filters are included with examples, the concepts of filtering based on fractional-order calculus are applied to the complementary filter, and the efficacy of non-integer-order filtering on systems with non-Gaussian noise is explored with good success.

Keywords Complementary filter · Unmanned aerial vehicle · Fractional-order calculus · Fractional-order filtering · Alpha-stable · Non-Gaussian · Sensor fusion · Navigation · Vertical take-off and landing (VTOL)

C. Coopmans (✉)
Center for Self-Organizing and Intelligent Systems (CSOIS), Utah State University, Logan, UT 84322, USA
e-mail: c.r.coopmans@ieee.org

A. M. Jensen
Utah Water Research Laboratory, Utah State University, Logan, UT 84322, USA
e-mail: austin.jensen@usu.edu

Y. Chen
Mechatronics, Embedded Systems and Automation (MESA) Lab, University of California, Merced, Merced, CA 95343, USA
e-mail: yqchen@ieee.org

1 Introduction

Unmanned aerial systems (UASs) are becoming very popular in many military and law-enforcement scenarios due to their reliability, maneuverability, relatively low cost, and safety to operators. The Center for Self-Organizing and Intelligent Systems (CSOIS) at Utah State University has been developing small, very low cost UAs (Unmanned Aircrafts) for use in many civilian personal remote sensing (PRS) applications such as water resources (remote sensing of agriculture data, vegetation mapping), and other civilian applications such as road and building site inspection. New missions such as distributed wind measurement or boarder patrolling require many UASs acting as a cooperative group to enable new kinds of distributed data collection. The majority of the remote sensing work performed at CSOIS has been that of multispectral imagery–the combining of multiple spectrum image data such

as near-infrared [25] and thermal infrared [24, 47] with visible light to produce much better information.

To accomplish mission goals or to fly passengers to their destinations, all aircraft rely on sensors for the core of their navigational systems. During PRS flights, it is of critical importance to determine the attitude of the aircraft, for stable flight, and more importantly, for data quality. The knowledge of the states of the aircraft is used to post-process and merge raw collected data into contiguous, useful datasets such as maps. This process requires many different sensors (rate gyros, accelerometers, etc.) to be combined into a single set of states useful for flight and data.

Kalman or Kalman-like combining filters are the established solution for combining sensor data into navigation-ready data. Extended Kalman filter approaches allow non-linear models to be linearized and used with the Kalman techniques, however, they have proved difficult to apply to SUASs with low-cost, high-noise sensors [26], and even EKF-based techniques are known to give unsatisfactory results [44]. Complementary filters are not mathematically rigorous like the Kalman filter, and therefore are not well-suited for high-risk applications like space missions. However, compared to Kalman filtering, complementary filter techniques are less computationally intensive and more readily performed on small, low-power processing hardware ideal for small, low-cost UASs.

Due to their inherent advantages, enriching complementary filters with new ideas may be beneficial. One paradigm which is gaining momentum in research is that of fractional calculus. The idea of fractional calculus has been known since the development of the regular calculus, with the first reference probably being associated with letter between Leibniz and L'Hospital in 1695. Fractional-order calculus is experiencing a resurgence as applications are found for the fractional calculus' more physical representation of dynamics of the real world.

The links between fractional–order calculus and stable power-law statistics are also well known [21]. Power-law like are ubiquitous [34], and although Kalman-style power-law aware filters (such as the Kalman–Levy filter) have been considered in research, they are not well studied and have even higher mathematical complexity compared to standard Kalman techniques [20]. Complimentary filters work without assuming Gaussian noise statistics, however, and are applicable to a wider variety of sensor hardware like commonly-available MEMS devices with longer-tail noise tendencies [29]. Since complementary filters require less computational power, they couple well with low-cost MEMs sensors and microcontrollers. Fractional-order filters are being implemented in other mechatronic applications such as lithography [12] with good success.

This study illustrates how different complementary filters are derived. Examples of each type of filter are simulated to show how they work and to make comparisons. The frequency domain complementary filter is described first in Section 2. Then examples of state space complementary filters are given in Section 3. Fractional-order complementary filters are included in Section 4, and Section 5 presents guidelines that describe the best situations to use complementary filters and conclusions are discussed in Section 6.

1.1 AggieAir Platform

AggieAir [16, 17] is a small, low-cost, autonomous, multispectral remote sensing platform [25], which has been developed over the last few years at CSOIS at USU. Work has begun on various applications through the AggieAir service center at the Utah Water Research Laboratory (UWRL) at USU. AggieAir utilizes both vertical takeoff and landing (VTOL) and fixed-wing platforms. As an example of AggieAir UAVs, a current hexarotor platform is shown in Fig. 1, and a current fixed-wing platform is shown in Fig. 2. For flight control, the open-source Paparazzi autopilot [1] is used for all platforms, with low-cost electronics and navigation sensors, while maintaining excellent flight characteristics and reliability [18].

The avionics of AggieAir's low cost UASs consist of an Inertial Navigation Unit (IMU), which measures acceleration, angular rate and magnetic field in three axis, Attitude Heading and Reference System (AHRS) which combines IMU measurements and provides attitude estimation, and a GPS sensor providing absolute position

Fig. 1 AggieAir Multirotor Platform—Hexarotor, ready for an indoor flight

Fig. 2 AggieAir Fixedwing Platform—Minion, during landing maneuver

altimeter (altitude above mean sea level), as well as pressure sensors for precise altitude estimation relative to a certain setpoint. Optionally an GPS Inertial Navigation System (GPS/INS) which combines measurements from all aforementioned sensors are fused together to estimate attitude and position can be used instead of AHRS [8].

In addition, a data radio transmitter/receiver is necessary for telemetry and remote control. The autopilot unit runs control loops on-board the UAS and controls the actuators to keep the desired the attitude and altitude as well as flight plan execution. Optionally a safety copilot, black box memory and payload can be added [18]. An overview of AggieAir system is shown in Fig. 3.

The control loops of a small UAS consist of attitude control, altitude control and position control, as shown in Fig. 4. The attitude controller controls the UAS's orientation, and uses IMU/AHRS to close the feedback loop. An altitude controller typically combines measurements from a pressure sensor and GPS altitude. Ultrasonic and laser altimeters are can be used as well. The position controller navigates the UAS in the airspace according to the mission requirements or safety copilot/operator input. Attitude and altitude controllers feed commands to the actuators, whereas position control calculates the desired altitude and orientation.

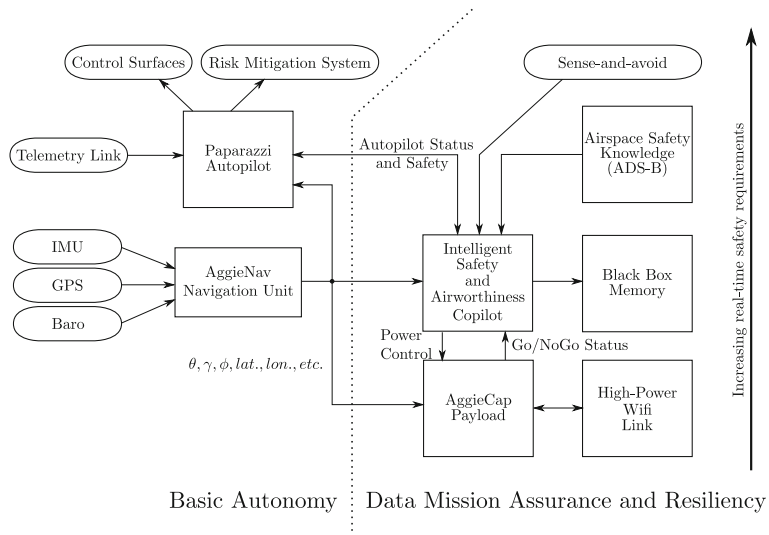

Fig. 3 AggieAir platform system diagram

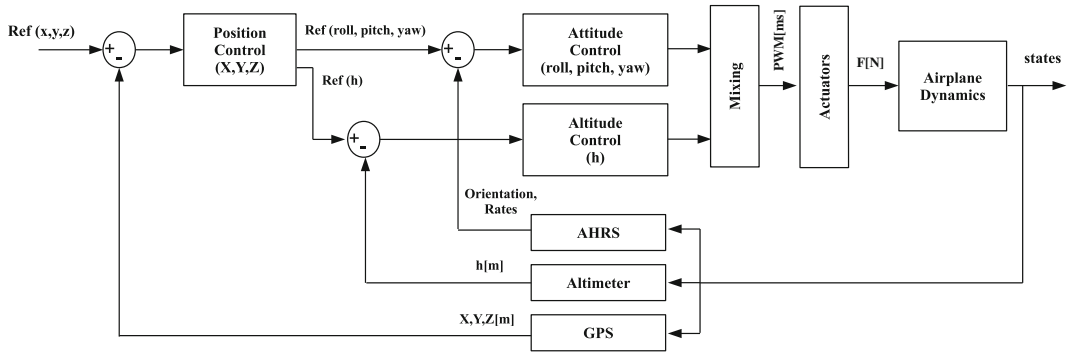

Fig. 4 General UAS flight control loops

1.2 Sensors and Navigation

For small UAVs targeted toward remote sensing, the navigation sensor suite determines much about the usefulness and capabilities of such a system, and is mostly limited because of the relatively high cost of high-quality navigational sensors and equipment.

Although technology is always improving, the options for high-quality, low-cost miniature attitude navigation sensors are few; many inexpensive, small fixed-wing UAVs use infrared thermopiles to sense the relative heat differential from the black body radiation of the Earth's surface. While this technique does work, it is not accurate enough for some remote measurement tasks and has problems when flying near large land features such as mountains and through valleys. Combined with a modern civilian GPS receiver, navigation is possible with these sensors, but applications in acquiring scientific data requires higher accuracy in attitude estimation.

Inertial measurement units with roll-rates and accelerometers are the standard sensor for attitude determination in flight. Several integrated solutions exist for navigation in small UASs, most of which use a Kalman or other state-estimation filter of some kind to provide a high-accuracy estimation of the current position and attitude of the system at a given instant. While these systems work well for their intended applications, even the academic prices are prohibitive for integration into inexpensive UAVs. Additionally, the source code is not made available, and users of the systems are forced to accept the filter/algorithm performance of the systems as they are given.

In any navigation system, performance and reliability are primary design drivers. In the world of small UAVs, size, weight and price are also of very high importance. Recently, due to the high-availability of low-cost sensing chips, many consumer-level devices such as Apple's iPhones, Nintendo Wii and Sony PlayStation 3 have integrated accelerometers into their hardware for more immersive user-experiences. Fully integrated 6-degree-of-freedom chips are being produced by Invensense, and other companies who target the consumer motion interface segments of the market. These sensors work well for static human motion applications, and not as well for dynamic applications such as aerial robotics.

Many organizations are producing IMUs for low-cost hobbyist-level (i.e., under ~$200USD) UAV flight such as Sparkfun, DIYDrones, etc. [13] based on complementary filters. These products are good enough for flight (and basic data collection in some cases), but with current data filtering techniques it is not possible to derive high-quality data from inexpensive sensor systems due to non-linearities, relatively poor noise performance, and poor temperature calibration [49].

1.3 Kalman Filtering for Small UASs

Estimating the orientation of the aircraft is a very important part of a UAS. Commonly a Kalman filter is used [11, 19, 26, 27, 43] and combines information from multiple sensors and models to estimate the orientation and variance. Kalman filters are model based and require system models to propagate state estimates. When the Kalman Filter receives measurements, it uses those

measurements and their models to update state estimates. One requirement of the Standard Kalman Filter is that these models must be linear. The Extended Kalman Filter does not share this same requirement and can be used when the models are non-linear. However the Extended Kalman Filter linearizes the models in the operation of the filter and assumes that the state estimates will not deviate far from the nominal solution. Knowledge about the noise attached to these models is also necessary to design a Kalman Filter, and most Kalman Filters assume that this noise is Gaussian. These assumptions make Kalman filters difficult to use with with small, low-quality inertial sensors due to the non-linearity and non-Gaussian characteristics of these sensors [23, 30]. In these cases, complementary filters are often used [6, 22, 44] because no assumptions are made about linearity and noise statistics [10].

1.4 Complementary Filters

The basic idea of a complementary filter is to take two or more sensors, filter out the unreliable frequencies for each sensor, and combine the filtered outputs to get a better estimate throughout the entire bandwidth of the system. To achieve this, the sensors included in the filter should complement each other by performing better over different parts of the system bandwidth than the other sensors. For example, one sensor could have reliable data at high frequencies and unreliable data at low frequencies. To complement this sensor, one or more sensors should be added to the filter that have reliable low frequency data. An example of two sensors that complement each other are an accelerometer and gyro. The gyro is reliable at high frequencies while the accelerometer is reliable at lower frequencies [30]. The complementary filter filters out the unreliable parts of the frequency for each sensor and combines their output. Figure 5 shows a diagram of a simple complementary filter with two sensors.

Complementary filters were first introduced in a patent in 1951 [52]. The patent describes an automated steering system for keeping a manned aircraft on a proper flight path during landing using the Instrument Landing Approach System (ILAS) along with a gyro-stabilized accelerometer. The ILAS was used to measure the rate of change between the distance from the aircraft and the desired path, and the gyro-stabilized accelerometer was used to measure changes in heading. The ILAS had reliable low frequency data but unreliable high frequency data, while the accelerometer had reliable high frequency data. Therefore, a complementary filter was used to combine this data, although the term "complementary filter" was not used. This term was coined in a journal paper in 1953 that describes a similar automated steering system [2]. The complementary filters in [52] and [2] were both designed in the frequency domain and realized with simple RC circuits.

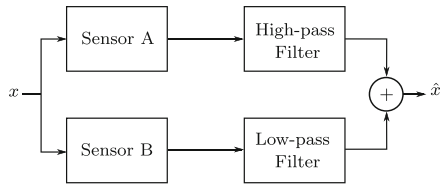

Fig. 5 Simple complementary filter diagram

Many other applications for the Frequency Domain Complementary Filter (FDCF) were presented after their introduction. Shaw and Srinivasan [46] used a complementary filter to combine low frequency position data from strain sensors and high frequency data from an accelerometer to estimate the position of the end of a beam. Zimmermann and Sulzer [53] used low frequency data from an inclinometer and high frequency accelerometer data to measure orientation. Baerveldt and Klang [6] introduced a similar system to measure orientation for an autonomous helicopter with an inclinometer and a gyro. Roberts et al. [44] used an accelerometer and a gyro to measure 3D orientation.

Eventually researchers began to design complementary filters in state space due to their advantages with multiple-input multiple-output systems, realization in digital systems, and closed loop control designs. A common application of the State Space Complementary Filter (SSCF) is to estimate the orientation of a rigid body. Bachmann et al. [3–5] used such a complementary filter based on quaternions to track the orientation of robotic flexible links. Quaternions are used

to represent orientation because they represent the axis and the rotation angle directly without singularities [45]. Instead of using quaternions to represent orientation, Mahony et al. [30] introduced a direct and passive complementary filter using a rotation matrix in the special orthogonal group, SO(3) (also referred to as a direct cosine matrix (DCM) [39], or attitude matrix [45]). Although the design of the filter was carried out using the SO(3), Mahony et al. [31] recommended that realization be done with quaternions. Hamel and Mahony [22] introduced another type of complementary filter based on SO(3), called the explicit complementary filter.

2 Frequency Domain Complementary Filters

To illustrate how a frequency-domain complementary filter works, assume that two sensors complement each other and can be used to measure a signal x. Both of these sensors can be modeled and have transfer functions $H_1(s)$ and $H_2(s)$. According to the complementary filter design, the unreliable frequencies of each sensor are filtered out by passing the outputs through filters $G_1(s)$ and $G_2(s)$. Figure 6 shows a block diagram of this system [6, 40].

The objective of the estimator is to find an estimate of x ($\hat{x}$) such that $\hat{x} = x$. This is possible, according to the block diagram in Fig. 6, if the transfer functions $G_1(s)$ and $G_2(s)$ are designed according to the following equation:

$$H_1(s)G_1(s) + H_2(s)G_2(s) = 1, \quad \forall s. \tag{1}$$

If $H_1(s)$ and $H_2(s)$ are known, they can be used with Eq. 1 to find $G_1(s)$ and $G_2(s)$. If $H_1(s)$ and $H_2(s)$ are not known, a model-free approach can be used which assumes that $H_1(s)$ and $H_2(s)$ are both ideal ($H_1(s) = H_2(s) = 1$). Instead of specifically designing $G_1(s)$ and $G_2(s)$ based on the sensor models, $G_1(s)$ and $G_2(s)$ are set as generic filters and tuned to minimize the error ($e = x - \hat{x}$).

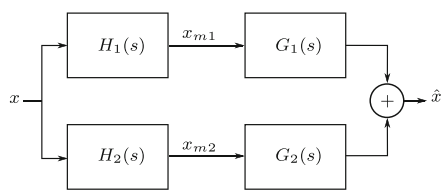

Fig. 6 Frequency domain complementary filter

With $H_1(s) = H_2(s) = 1$, Eq. 1 becomes the following:

$$G_1(s) + G_2(s) = 1, \quad \forall s, \tag{2}$$

and is used as a constraint when choosing filters for $G_1(s)$ and $G_2(s)$.

While using the model-free approach, one might choose the second order filters in Eqs. 3 and 4 for $G_1(s)$ and $G_2(s)$. Since ω_0 determines where the filters are cut-off, it is used as a tuning parameter. Figure 7 shows a Bode plot of $G_1(s)$ and $G_2(s)$ with $\omega_0 = 1$. If ω_0 is reduced, more of $H_1(s)$ is filtered out and more of $H_2(s)$ is allowed to pass through ($H_2(s)$ dominant). If ω_0 is increased, more of $H_2(s)$ is filtered out and more of $H_1(s)$ is allowed to pass through ($H_1(s)$ dominant). A well-designed filter will have a value for ω_0 such that the best parts of both $H_1(s)$ and $H_2(s)$ are allowed to passed through while the unreliable parts are filtered out.

$$G_1(s) = \frac{2\omega_0 s + \omega_0^2}{(s+\omega_0)^2}. \tag{3}$$

$$G_2(s) = \frac{s^2}{(s+\omega_0)^2}. \tag{4}$$

2.0.1 FDCF Example—Model-free Second Order Filter

A model-free FDCF with second order filters can be used to combine the outputs of an inclinometer and a gyroscope to measure orientation. An inclinometer is a general term given to devices that directly measure orientation; one example is an accelerometer. The accelerometer measures orientation by the acceleration due to gravity. In general, inclinometers have a slow response time and will filter out high frequency movement. A gyro measures angular rate, which is converted to orientation by integration. While the gyro does well at high frequencies, the inherent noise and integration introduces drift. The complementary filter improves the orientation estimate by combining the reliable high frequency data from the gyro and the low frequency data from the inclinometer.

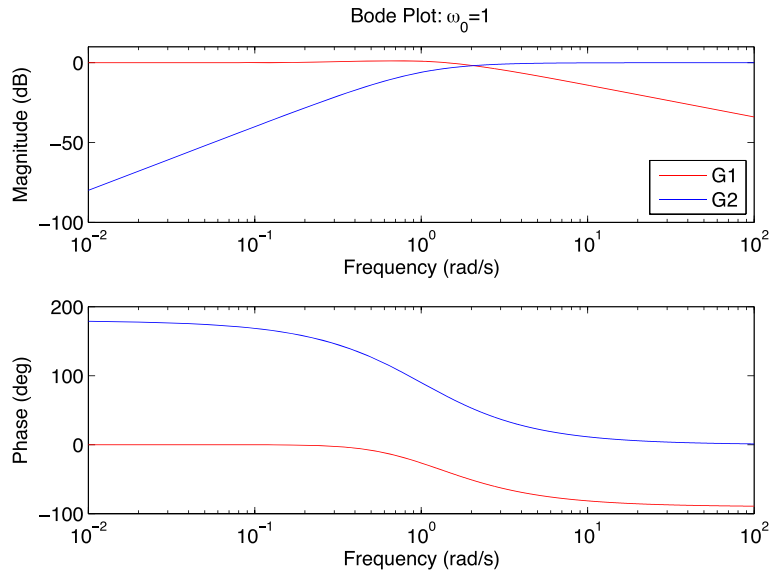

Fig. 7 Bode plots of $G_1(s)$ and $G_2(s)$

Simulink is used to test the Second Order FDCF with the inclinometer and gyro. As shown in the simulink model in Fig. 8, the inclinometer is modeled as the transfer function in Eq. 5 [6]. The gyro is modeled as the derivative of the actual orientation plus a bias. Noise is also added to the gyro before the signal is integrated to get orientation. The output of the sensors are then passed through the filters from Eqs. 3 and 4 and combined to get the orientation estimate.

$$H_1(s) = \frac{1.88}{s + 1.88}. \tag{5}$$

The input orientation to the simulation is a chirp signal that produces a sine wave between ±10 degrees at frequencies between 0.05 Hz and 1 Hz. At the beginning of the simulation, the sine wave will start at 1Hz and gradually decrease to 0.05 Hz after 100 s. At that point, the frequency will gradually increase until the end of the simulation.

Figures 9 and 10 show the response of the inclinometer and gyro to the input chirp signal. As expected, the inclinometer cannot track the input at high frequencies. However, as the frequency is reduced, the inclinometer is more capable of tracking the sine wave. The output of the gyro is also expected; it tracks the input well but drifts away from the actual orientation at 1 degree per second.

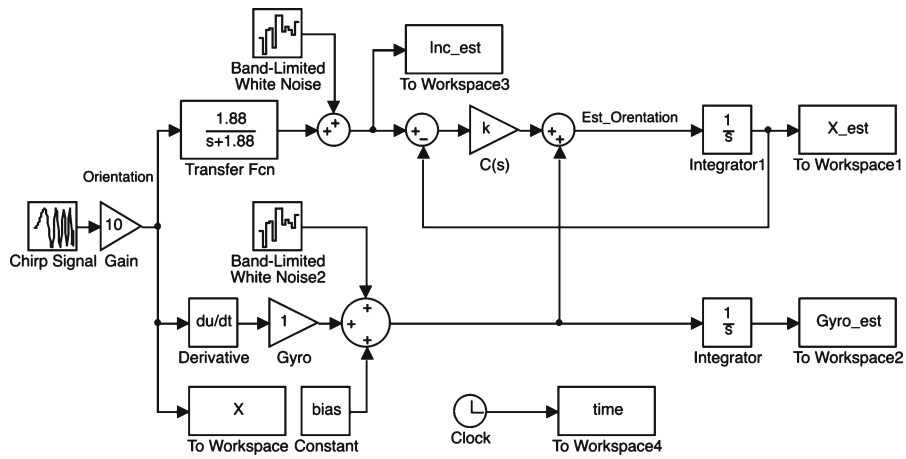

Fig. 8 Simulink model of complementary filter—model-free design

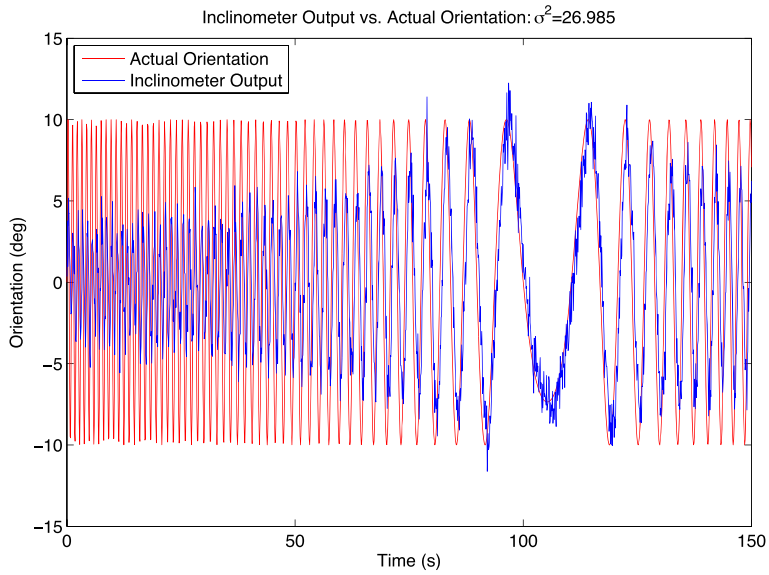

Fig. 9 Response of the inclinometer to the input chirp signal

The filter is tuned by finding the optimal value of ω_0 that minimizes the error e. This is done by running multiple simulations with varying values of ω_0 (0.01 rad/s to 0.5 rad/s). At the end of each simulation, the squared error and the variance are calculated for each value of ω_0. Figure 11 shows the result of these simulations. The lowest variance is $\sigma^2 = 2.23$ with an ω_0 of 0.22 rad/s. Figures 12 and 13 show plots of the filter output (estimated orientation) and the squared error with this optimal frequency.

While exploring the concept of a complementary filter, it is also worthwhile to look at the filter output at non-optimal frequencies. As Fig. 11 explains, if ω_0 is too high, the inclinometer will dominate the output of the filter. If ω_0 is too low, the gyro will dominate the output of the filter. Figures 14 and 15 show the filter output and error plots when ω_0 is too high and the output is dominated by the inclinometer. Notice how similar the output plot matches the output of the inclinometer in Fig. 9. Figures 16 and 17 show the

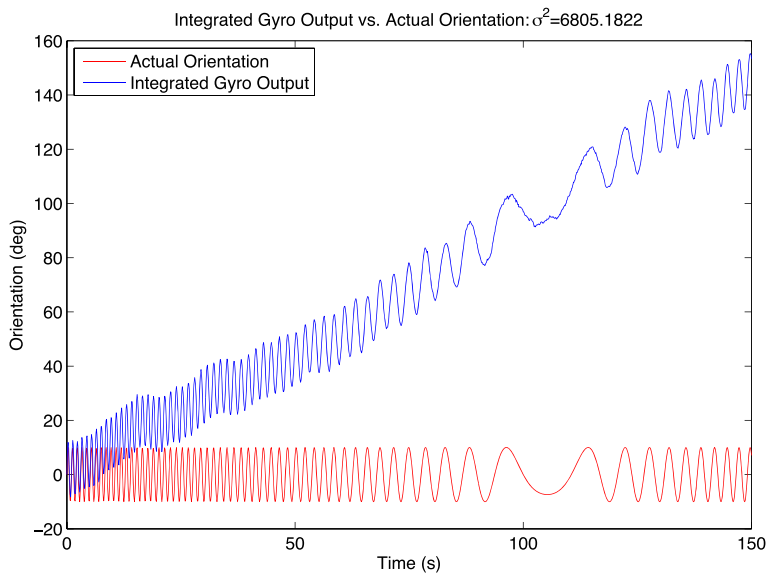

Fig. 10 Response of the gyro to the input chirp signal

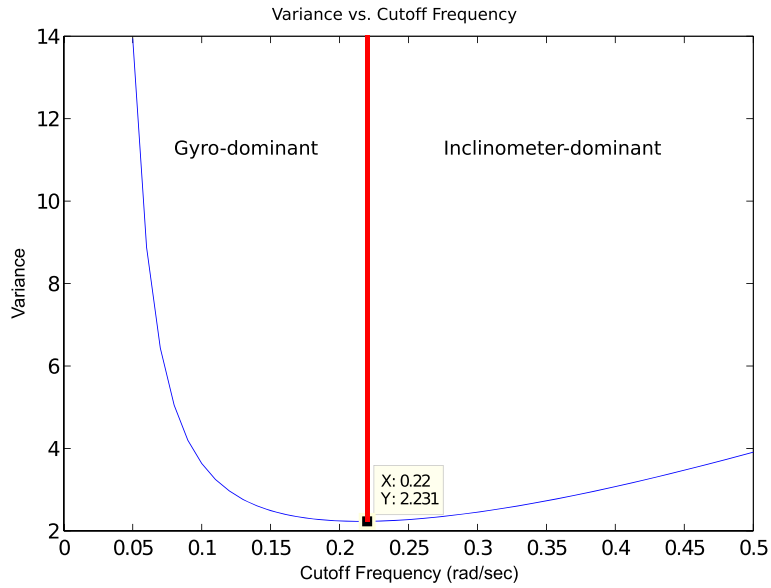

Fig. 11 Variance of the error vs. cutoff frequency (ω_0)

filter output and error plots when ω_0 is too low and the output is dominated by the gyro. These gyro dominated plots also show similarities to the gyro output in Fig. 10.

2.0.2 Other FDCF Design Options

The previous example simulated for this study shows how a model-free FDCF with second order filters can be used to combine the output of two sensors to get a better estimate of orientation. Other design options for FDCFs include more complex, higher order filters and filters based on the sensor models. Some of these options may achieve better performance than was shown in the previous example [6].

3 State Space Complementary Filters

The complementary filter can be interpreted in state space form in order to easily realize the com-

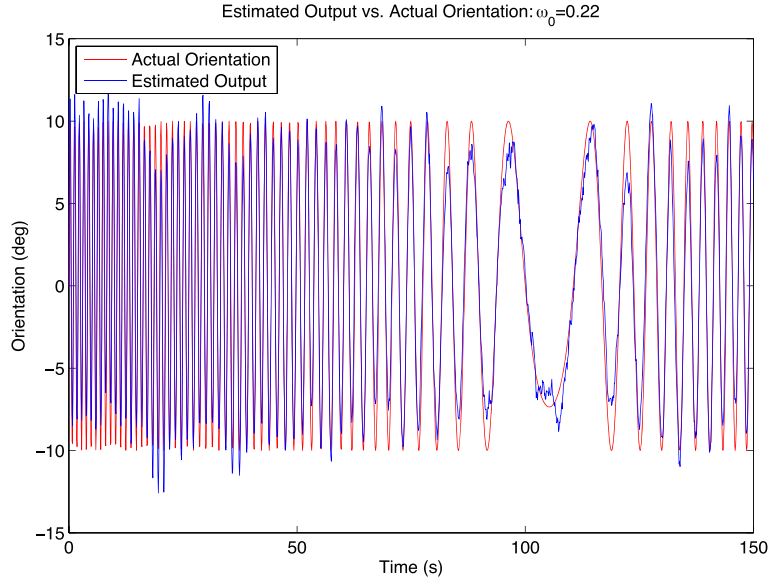

Fig. 12 Estimated orientation vs. actual orientation at $\omega_0 = 0.22$ rad/s (Optimal Frequency)

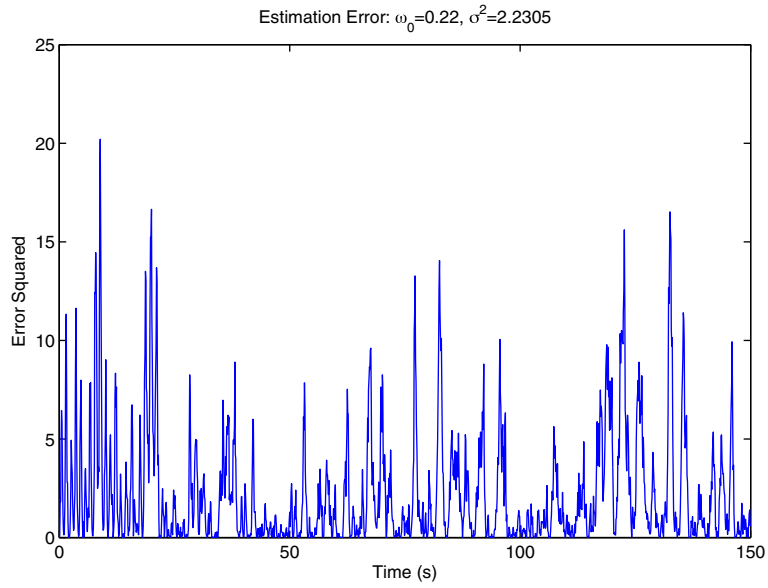

Fig. 13 Squared error for $\omega_0 = 0.22$ rad/s (Optimal Frequency)

plementary filter with digital systems, implement multiple-input multiple-output systems, and use classical control theory for filter design [30, 37]. Figure 18 illustrates this conversion with an example of the frequency domain complimentary filter where ϕ_i and ϕ_g are the outputs from the inclinometer and the gyro, $G_i(s)$ and $G_g(s)$ are the filters for the inclinometer and gyro, and $\hat{\phi}$ is the estimate of ϕ.

To be a complementary filter, $G_i(s) + G_g(s)$ must equal 1 (as shown in Eq. 2). Therefore $G_i(s)$ and $G_g(s)$ could be set as the following:

$$G_i(s) = \frac{C(s)}{C(s) + s}, \tag{6}$$

$$G_g(s) = \frac{s}{C(s) + s}. \tag{7}$$

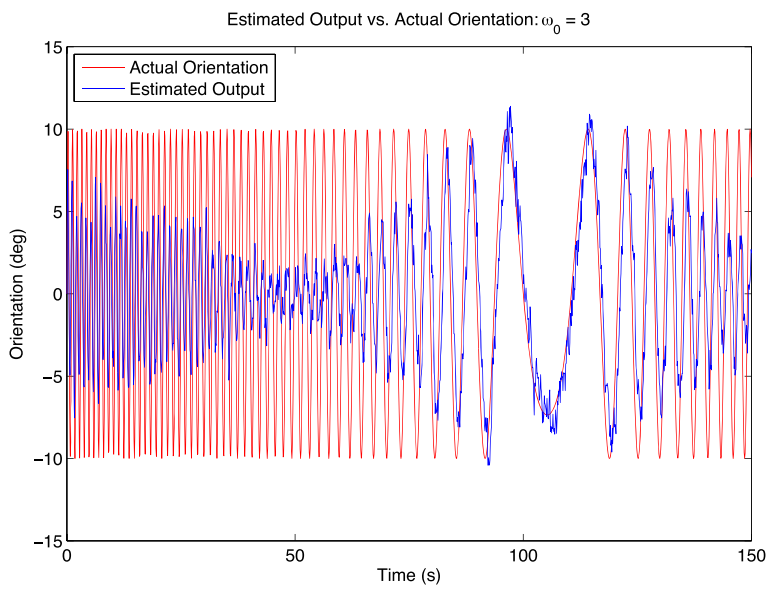

Fig. 14 Estimated orientation vs. actual orientation at $\omega_0 = 3$ rad/s (Inclinometer Dominant)

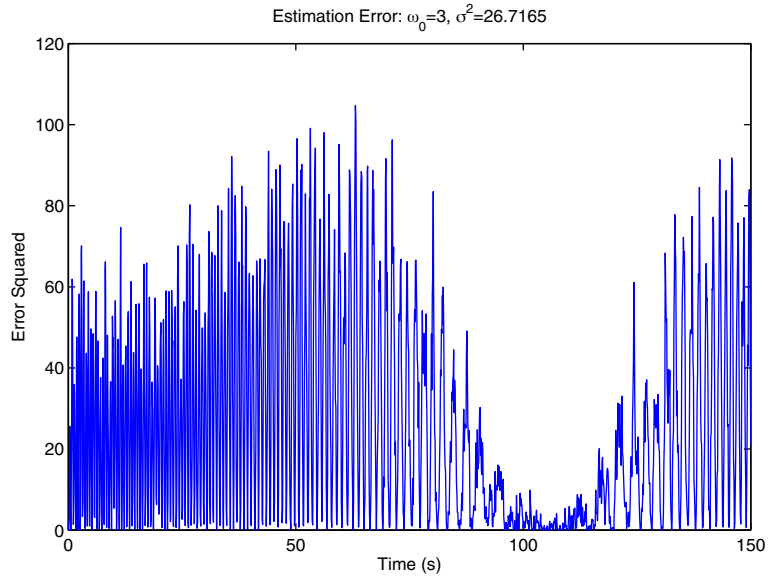

Fig. 15 Squared error for $\omega_0 = 3$ rad/s (Inclinometer Dominant)

According to the diagram in Fig. 18 and the definitions of $G_i(s)$ and $G_g(s)$, $\hat{\phi}$ is defined as

$$\begin{aligned}\hat{\phi} &= \phi_i \frac{C(s)}{C(s)+s} + \frac{\phi_g}{s}\frac{s}{C(s)+s},\\ \hat{\phi} &= \left(\phi_i C(s)s + \phi_g - C(s)\hat{\phi}\right)\frac{1}{s},\\ s\hat{\phi} &= (\phi_i - \hat{\phi})C(s) + \phi_g. \end{aligned} \tag{8}$$

Equation 8 represents the frequency domain complementary filter in the closed-loop form as displayed in Fig. 19. With this design, classical closed-loop control theory can be used to design the complementary filter.

After choosing a controller, Eq. 8 can be converted to state space. Using a gain controller, P, Eq. 9 shows the state space representation of a

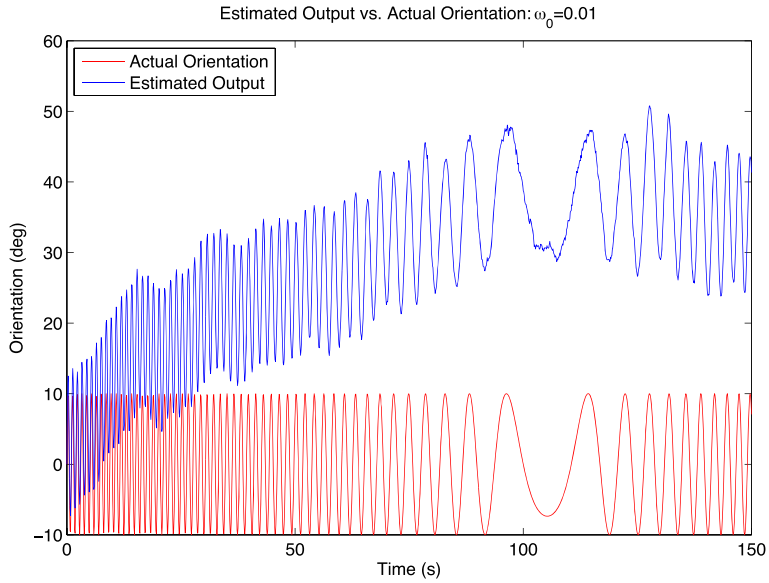

Fig. 16 Estimated orientation vs. actual orientation at $\omega_0 = 0.01$ rad/s (Gyro Dominant)

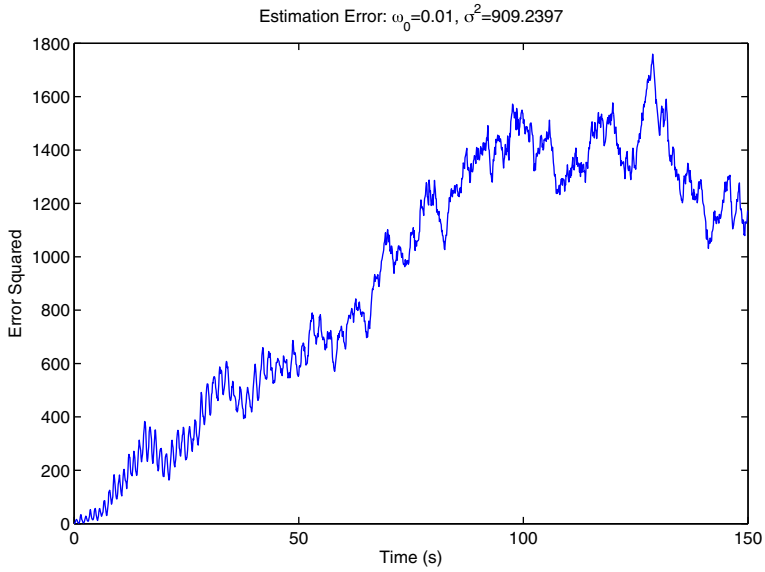

Fig. 17 Squared error for $\omega_0 = 0.01$ rad/s (Gyro Dominant)

complementary filter with $\hat{\phi}$ set as the state space variable x.

$$\dot{x} = (\phi_i - x)P + \phi_g. \tag{9}$$

Additionally, classical closed-loop control theory can now be used to design the complementary filter. Since there is a good deal of established research on application of fractional calculus in closed-loop control [33], it is a simple matter to change the integer-order controller to a fractional-order one as seen in Section 4.

3.1 SSCF Example—Using a Gain Controller

To test the SSCF from Eq. 9, the simulator from Section 2.0.1 was used. After running this simulation multiple times for different values of P, they are plotted with their respective error variance to find the gain P with the lowest error. Figure 20 shows this plot and a minimum variance of $\sigma^2 = 4.15$ with a gain of 0.84. Figures 21 and 22 show the filter output and squared error plots using the optimal gain.

Even though it was subjected to the same input, the performance of this filter was not as good as the frequency domain filter designed in Section 2. This could be because of constant bias in the gyro. Introducing an integrator in the controller could improve the performance by removing this bias.

3.2 SSCF Example—Using a PI Controller

After adding an integrator to the controller $C(s)$, Eq. 8 can be written as shown below where P is constant gain and I is integrator gain.

$$s\hat{\phi} = (\phi_i - \hat{\phi})(P + I/s) + \phi_g,$$
$$s\hat{\phi} = (\phi_i - \hat{\phi})P + (\phi_i - \hat{\phi})I/s + \phi_g. \tag{10}$$

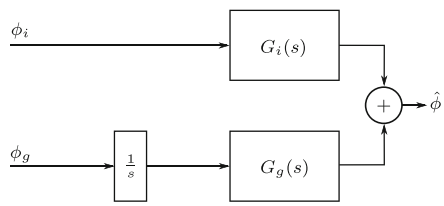

Fig. 18 Frequency domain complementary filter

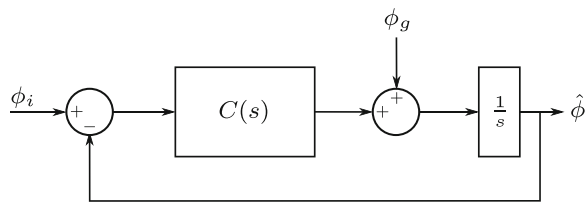

Fig. 19 Closed-loop complementary filter system

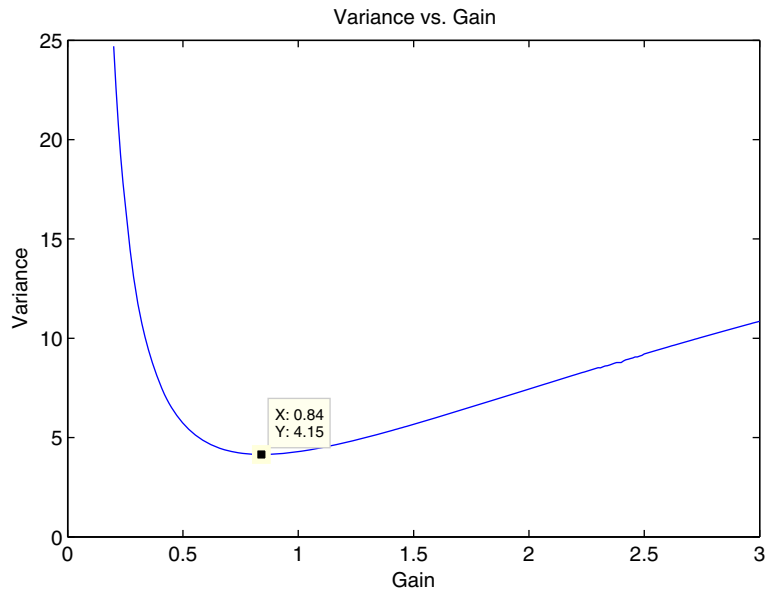

Fig. 20 Variance of the error vs. controller gain (P) for SSCF

The term $(\phi_i - \hat{\phi})I/s$ is compensation for the bias and can be set as one of the state variables x_2. x_1 will remain equal to the estimated angle $\hat{\phi}$.

$$\dot{x_1} = (\phi_i - x_1)P + x_2 + \phi_g,$$
$$\dot{x_2} = (\phi_i - x_1)I. \tag{11}$$

Notice the similarities between Eqs. 11 and 9. Equation 11 can now be rearranged into its matrix representation (Eq. 12) where b is the gyro bias. The -1 found in the 'C' matrix is negative in order to cancel out the gyro bias.

$$\begin{bmatrix} \dot{x_1} \\ \dot{x_2} \end{bmatrix} = \begin{bmatrix} -P & 1 \\ -I & 0 \end{bmatrix} \begin{bmatrix} x_1 \\ x_2 \end{bmatrix} + \begin{bmatrix} P & 1 \\ I & 0 \end{bmatrix} \begin{bmatrix} \phi_i \\ \phi_g \end{bmatrix},$$
$$\begin{bmatrix} \hat{\phi} \\ \hat{b} \end{bmatrix} = \begin{bmatrix} 1 & 0 \\ 0 & -1 \end{bmatrix} \begin{bmatrix} x_1 \\ x_2 \end{bmatrix}. \tag{12}$$

Figure 23 shows the realization of Eq. 12 in Simulink. This model was used with the same input signal and sensor models from the simulation

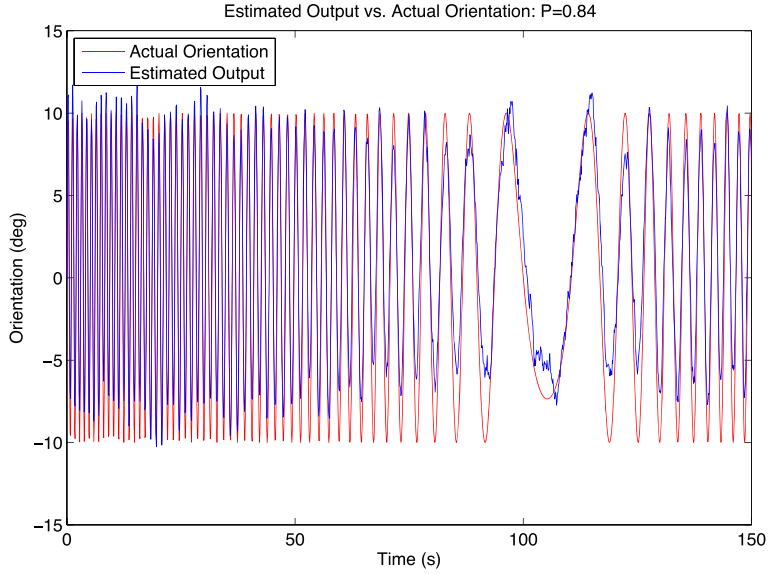

Fig. 21 Estimated orientation vs. actual orientation with $P = 0.84$ (Optimal Gain)

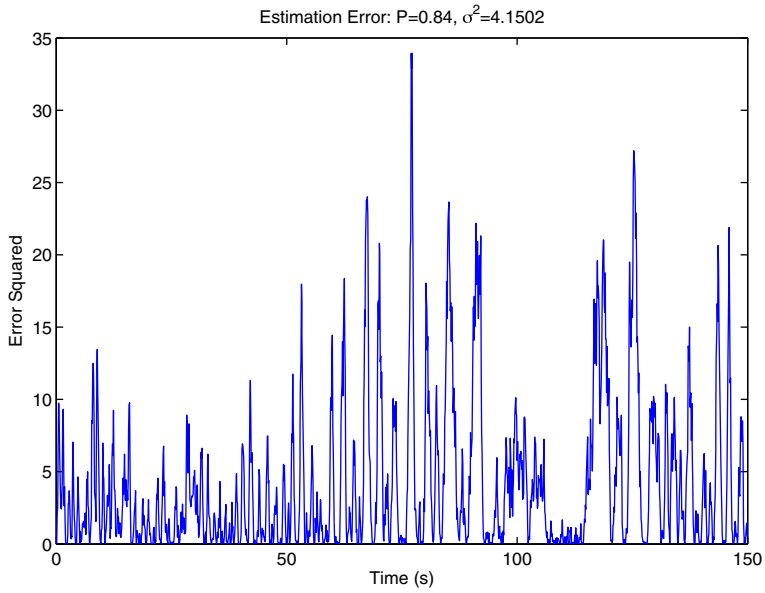

Fig. 22 Squared error for $P = 0.84$ (Optimal Gain)

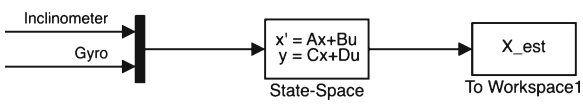

Fig. 23 Simulink model of state space complementary filter

in Section 2.0.1. Multiple values of P and I were simulated, the variance of the error was found, and the contour plot in Fig. 24 was generated to find the optimal values for P and I that minimize the variance of the error. As shown in Fig. 24, the optimal values for P and I in this example are 0.44 and 0.048, respectively, with a variance of $\sigma^2 = 2.31$.

Figures 25 and 26 show the output of the filter with optimal gains. With a variance of $\sigma^2 = 2.31$,

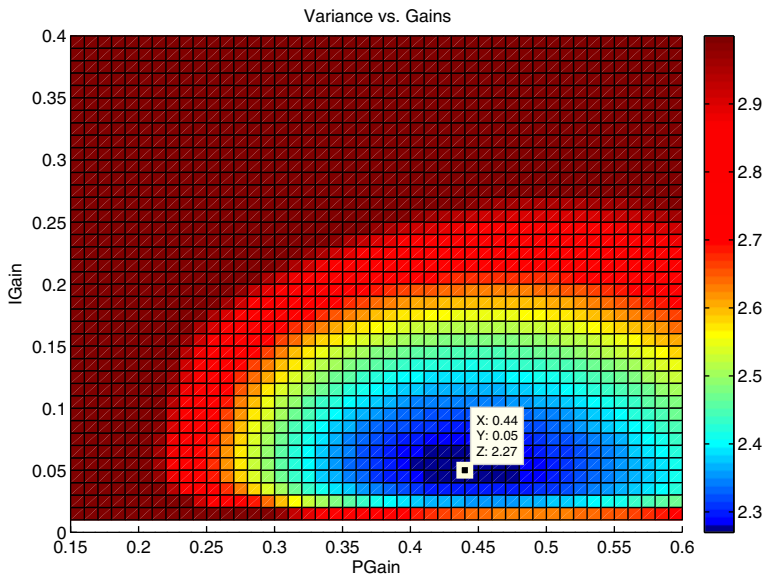

Fig. 24 Variance of the error vs. controller gains (P and I) for SSCF

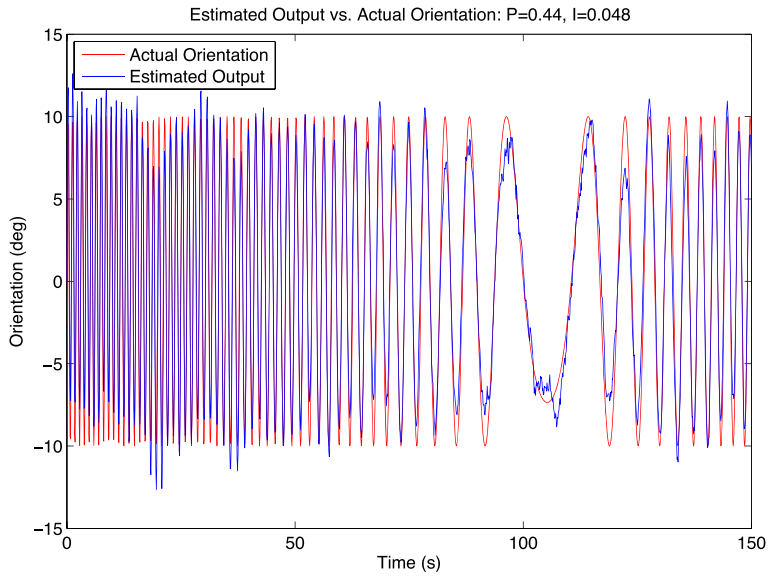

Fig. 25 Estimated orientation vs. actual orientation with $P = 0.44$ and $I = 0.048$ (Optimal PI Gains)

the performance of this filter is very similar to the performance of the frequency domain filter designed in Section 2. This similarity is expected. If the complementary filter from Eq. 12 were converted back into its frequency domain form shown in Fig. 18, the system would be identical to the second-order filters shown in Eqs. 3 and 4, where $P = 2\omega_0$ and $I = \omega_0^2$. Therefore, these two systems are equivalent. However, the state space system would be easier to implement using a digital computer. In addition, it is possible to estimate the bias in the state space system since it is added as an additional state. Figure 27 shows the estimated bias vs. the actual bias.

3.3 Other SSCF Design Options

Since the SSCF is derived using the closed-loop control version of the complementary filter, any other type of controller could be used to help

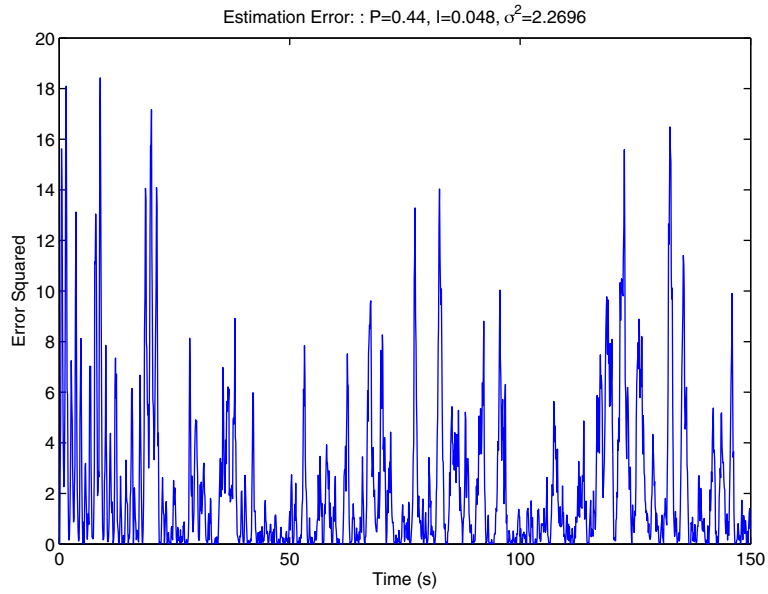

Fig. 26 Squared error for $P = 0.44$ and $I = 0.048$ (Optimal PI Gains)

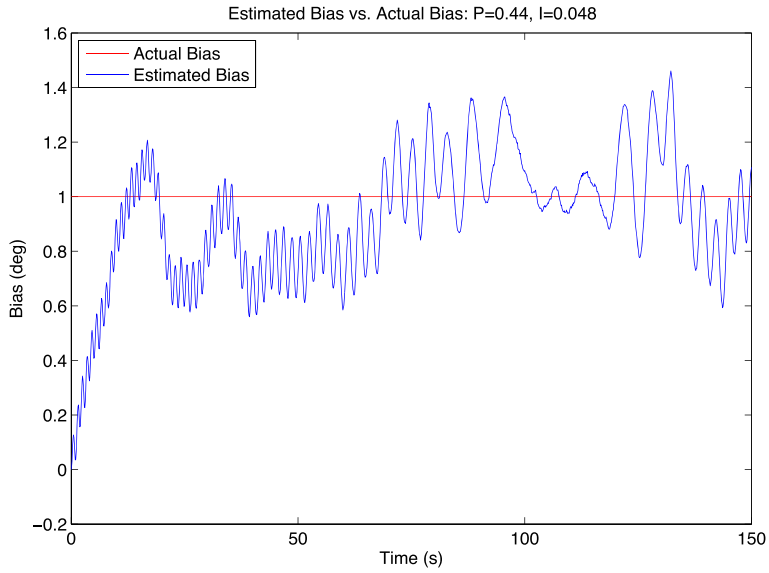

Fig. 27 Estimated Bias Plots for $P = 0.44$ and $I = 0.048$

improve the performance of the filter. For example, a full PID controller could possibly perform better in some systems than the PI controller. Other possibilities include model based controllers and fractional order controllers.

SSCFs are also used for multiple-input multiple-output systems. These include SSCFs to estimate three-dimensional orientation using Euler-angles, quaternions [3], and direct cosine matrices [32, 39]. Work has also been done on estimating position and velocity using complementary filters [7].

4 Fractional-Order Complementary Filters

4.1 Fractional-Order Calculus

The idea of fractional calculus has been known since the development of the regular calculus, with the first reference probably being associated with letter between Leibniz and L'Hospital in 1695.

Fractional calculus is a generalization of integration and differentiation to non-integer order fundamental operator ${}_aD_t^\alpha$, where a and t are the limits of the operation. The continuous integro-differential operator is defined as

$${}_aD_t^\alpha = \begin{cases} \dfrac{d^\alpha}{dt^\alpha} & : \alpha > 0, \\ 1 & : \alpha = 0, \\ \int_a^t (d\tau)^{-\alpha} & : \alpha < 0. \end{cases}$$

The two definitions used for the general fractional differintegral are the Grunwald-Letnikov (GL) definition and the Riemann–Liouville (RL) definition [36, 41]. The GL is given here

$${}_aD_t^\alpha f(t) = \lim_{h\to 0} h^{-\alpha} \sum_{j=0}^{[\frac{t-a}{h}]} (-1)^j \binom{\alpha}{j} f(t - jh), \quad (13)$$

where [.] means the integer part. The RL definition is given as

$${}_aD_t^\alpha f(t) = \frac{1}{\Gamma(n-\alpha)} \frac{d^n}{dt^n} \int_a^t \frac{f(\tau)}{(t-\tau)^{\alpha-n+1}} d\tau, \quad (14)$$

for $(n-1 < \alpha < n)$ and where $\Gamma(.)$ is the *Gamma* function.

The Laplace transform method is used for solving engineering problems. The formula for the Laplace transform of the RL fractional derivative (14) has the form [41]:

$$\int_0^\infty e^{-st}\, {}_0D_t^\alpha f(t)\, dt$$

$$= s^\alpha F(s) - \sum_{k=0}^{n-1} s^k \; {}_0D_t^{\alpha-k-1} f(t)\big|_{t=0}, \quad (15)$$

for $(n-1 < \alpha \leq n)$, where $s \equiv j\omega$ denotes the Laplace operator.

Some others important properties of the fractional derivatives and integrals we can find in several existing works (e.g., [36, 41], etc.).

4.2 Fractional-Order Filtering

In order to implement fractional-order calculus in a real system, a practical approximation must be made. While it is possible to realize fractional-order elements in analog hardware–'passive' hardware devices for fractional-order integrator, such as fractances (e.g., RC transmission line circuit and Domino ladder network) [42] and Fractors [9], there exist some restrictions, since these devices are currently difficult to tune. An alternative feasible way to implement fractional-order operators and controllers is to use finite-dimensional integer-order transfer functions, or fractional-order signal processing.

The fractional-order differentiator and fractional-order integrator are fundamental building blocks for fractional-order signal processing. The transfer function of fractional-order integrator (FOI) is simply

$$G_{FOI}(s) = \frac{1}{s^{\alpha}}$$

where α is a positive real number. Without loss of generality, we only consider $0 < \alpha < 1$. The transfer function of fractional-order differentiator (FOD) is simply

$$G_{FOD}(s) = \frac{1}{G_{FOI}(s)} = s^{\alpha}.$$

In time domain, the impulse response of $G_{FOI}(s)$ is

$$h(t) = L^{-1}G_{FOI}(s) = \frac{t^{\alpha-1}}{\Gamma(\alpha)}, \quad t \geq 0.$$

Replacing α with $-\alpha$ will give the impulse response of fractional differentiator s^{α}.

A FOI or FOD is an infinite-dimensional system. So, when implemented digitally, it must be approximated with a finite-dimensional discrete transfer function. This is the so-called "discretization" problem of FOI or FOD [14]. We refer to [15, 28, 33] for excellent reviews and tutorials on discretization issues.

As said, an integer-order transfer function representation to a fractional-order operator s^{α} is infinite-dimensional. However, it should be pointed out that a band-limited implementation of fractional-order controller (FOC) is important in practice, i.e., the finite-dimensional approximation of the FOC should be done in a proper range of frequencies of practical interest [38]. Interestingly, the fractional-order α could even be a complex number as discussed in [38].

In this paper, the recursive frequency-space discretization techniques of Oustaloup et al. [38] are used. A generalized Oustaloup filter can be designed as

$$G_f(s) = K\prod_{k=1}^{N}\frac{s+\omega_k'}{s+\omega_k}, \tag{16}$$

where, the poles, zeroes and gain are evaluated from

$$\begin{aligned}\omega_k' &= \omega_b\,\omega_{\mathrm{u}}^{(2k-1-\gamma)/N},\\ \omega_k &= \omega_b\,\omega_{\mathrm{u}}^{(2k-1+\gamma)/N},\quad K = w_h^{\gamma},\end{aligned} \tag{17}$$

where $\omega_{\mathrm{u}} = \sqrt{\omega_{\mathrm{h}}/\omega_{\mathrm{b}}}$. The term "generalized" is used because N can be an odd or even integer.

To illustrate the method, the approximation of the fractional-order integrator of order 0.45 can be obtained. In this particular case, the orders of the approximation are selected as 4 and 5, respectively, with $\omega_{\mathrm{h}} = 1000$ rad/s and $\omega_{\mathrm{b}} = 0.01$ rad/s. Using MATLAB, from [48], $H_{\mathrm{Oust}}(s)$ approximations:

$$G_{O1} = \frac{0.04467s^4+21.45s^3+548.2s^2+783.2s+59.57}{s^4+131.5s^3+920.3s^2+360.1s+7.499},$$

and

$$G_{O2} = \frac{0.04467s^5+26.35s^4+1413s^3+7500s^2+3942s+188.4}{s^5+209.3s^4+3982s^3+7500s^2+1399s+23.71}.$$

The Bode plots are shown in Fig. 28. It can be seen that the Bode plots of the two filters are relatively close to that of the theoretical one over the frequency range of interest. It can be seen that the fitting quality is much superior to those obtained with continued fraction based approaches.

Detailed comparisons of different methods of FOI and FOD discritization can be found in Chapter 5 the 2012 book by Sheng et al. [48].

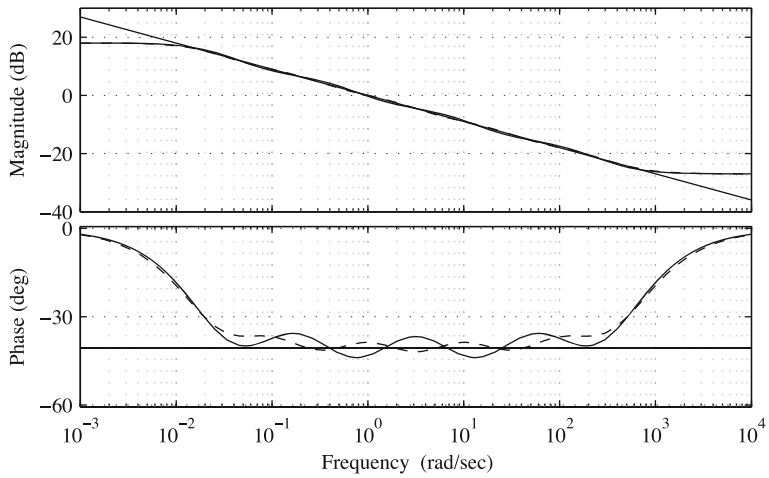

Fig. 28 Bode plots of $H_{\mathrm{Oust}}(s)$, corresponding to the approximation of a fractional-order integrator of order 0.45 with the Oustaloup method, with *solid lines* for G_{O1}, *dash lines* for G_{O2} and dotted lines for the theoretical Bode plot

4.3 Alpha-stable Noise

The probability distribution functions (PDFs) of the sensors used for small UAS navigation are very important to filter choice and tuning. Using the alpha-stable random distribution (ARD), a standard Gaussian PDF as well as a non-Gaussian PDF was used for simulation.

The ARD is usually denoted $S(\alpha_n, \beta, \gamma, \delta)$. Note that this α_n differs from the fractional-order α. Due to the ARD's nature, only in select cases can the PDF be written analytically, however, from [35], the characteristic function φ and the PDF can be determined by:

$$f(x) = \frac{1}{2\pi}\int_{-\infty}^{\infty} \varphi(t)e^{-ixt}\,dt,$$

where

$$\varphi(t;\mu,c,\alpha_n,\beta) = \exp\left[\, it\mu - |ct|^{\alpha_n}(1 - i\beta\,\mathrm{sgn}(t)\Phi)\right],$$

and

$$\Phi = \tan(\pi\alpha_n/2), \quad \alpha_n \neq 1.$$

The ARDs generalize many PDFs, for example, the well-known Gaussian PDF

$$f(x) = \frac{1}{\sigma\sqrt{2\pi}}e^{-\frac{(x-\mu)^2}{2\sigma^2}} \tag{18}$$

is conveniently produced by the ARD with $\alpha_n = 2$, $\gamma = \frac{\sigma}{\sqrt{2}}$. This means that the Gaussian distribution is encapsulated within the alpha-stable distribution, and a single function can be used to simulate both Gaussian and SRD noise cases.

For the purposes of this paper, the ARD was always used with $\alpha_n = 1.8$, and scale-parameter $\gamma = 1.3$. As seen in the plots such as Fig. 29, this generates noise sufficiently "spiky" (non-Gaussian) to be considered low-quality (i.e., low-cost). The effective PDFs of both of the distributions used are found in Fig. 30.

The differences in these PDFs can be clearly seen in Figs. 9 and 10, by comparison to Figs. 29 and 31.

4.4 Fractional-Order Complementary Filter Simulations

By their nature, integer-order and fractional-order controllers have different numbers of parameters and can be difficult to compare fairly. The experiments performed in this paper were as follows: the integer-order controller was simply a P (or constant-gain) controller. The fractional-order controller was I^{α} (single-term fractional with constant gain). This allows for nearly the same degrees of freedom in the simulation process and the most fair comparison. The block diagram for the example system is shown in Fig. 32. Since the fractional calculus encapsulates the integer-order calculus with proper choices of α, the same system diagram can be used for all the simulations. The P case is set when $\alpha = 0$.

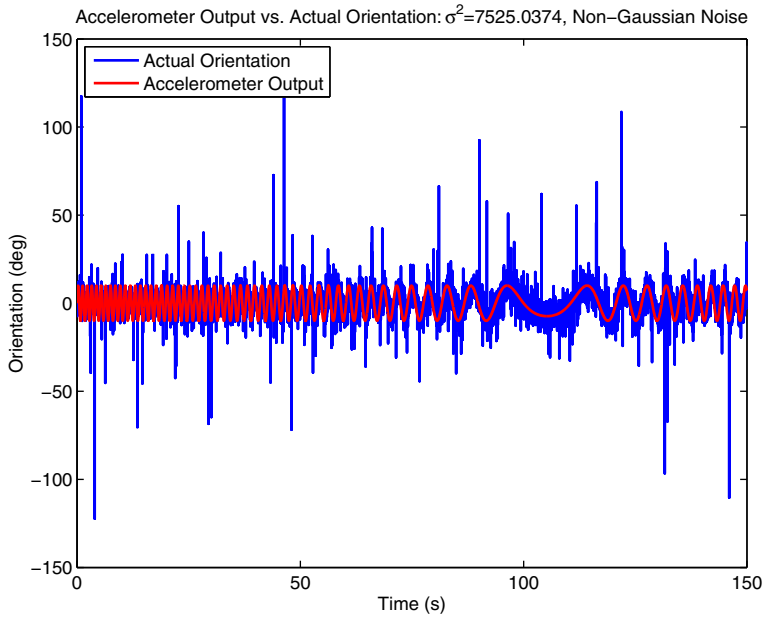

Fig. 29 Inclinometer signal with non-Gaussian noise

To accomplish numerical simulations of FOCFs, the following codes from MATLABCentral were used:

- *STBL: Alpha stable distributions for MATLAB* by Veillette [51] for ARD generation
- *ninteger* by Duarte Valrio [50] for fractional operator simulation

The *ninteger* package includes a full toolbox for simulation of fractional-order implementations in MATLAB Simulink. Due to its numerical reliability, the CRONE distretization (as in Section 4.2) was chosen for the I^{α} feedback term, with $\omega_b = 0.01$ rad/sec and $\omega_h = 1000$ rad/sec. Recall that negative values of α create an integrator-like operator.

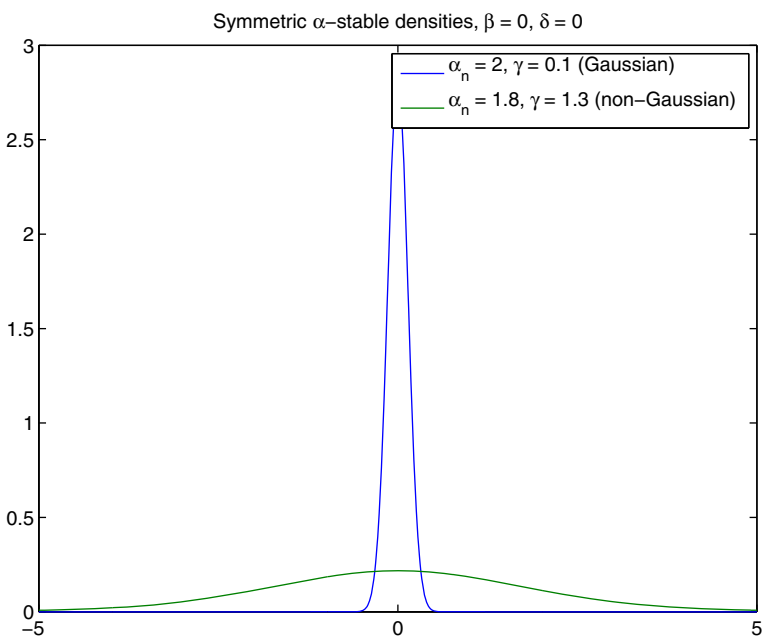

Fig. 30 Gaussian and non-Gaussian PDFs used in numerical simulations

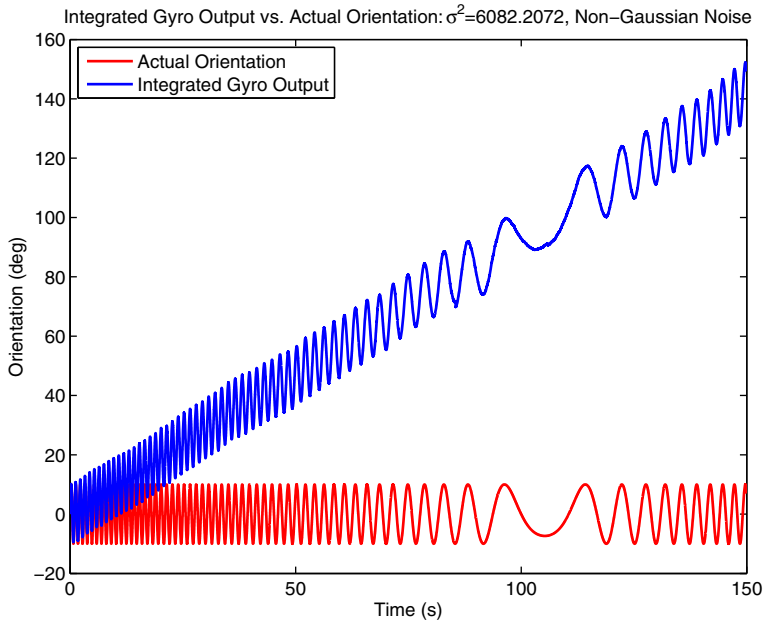

Fig. 31 Gyro signal with non-Gaussian noise and offset

4.5 Fractional-Order Complementary Filter Simulation Results

Five simulations were performed to investigate the performance of the system in question:

1. First, an integer system with a simple P controller was used. A range of gains was used and the variance tracked, to find the minimum. As seen in Fig. 33, this was $k = 0.75$, resulting in $\sigma^2 = 3.975$.
2. Then, this same simulation was performed with non-Gaussian noise, under which the system produced nearly the same plot (Fig. 34), however with the long waiting times (heavy-tailedness) involved with the ARD, the variance was not as consistent over the range of gains as the Gaussian case.

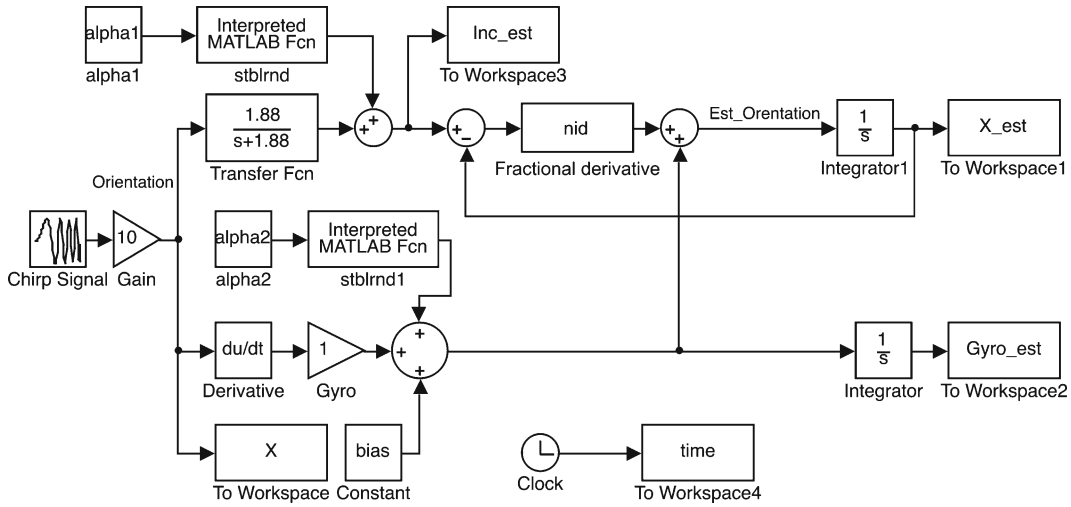

Fig. 32 Simulink model used for all simulations

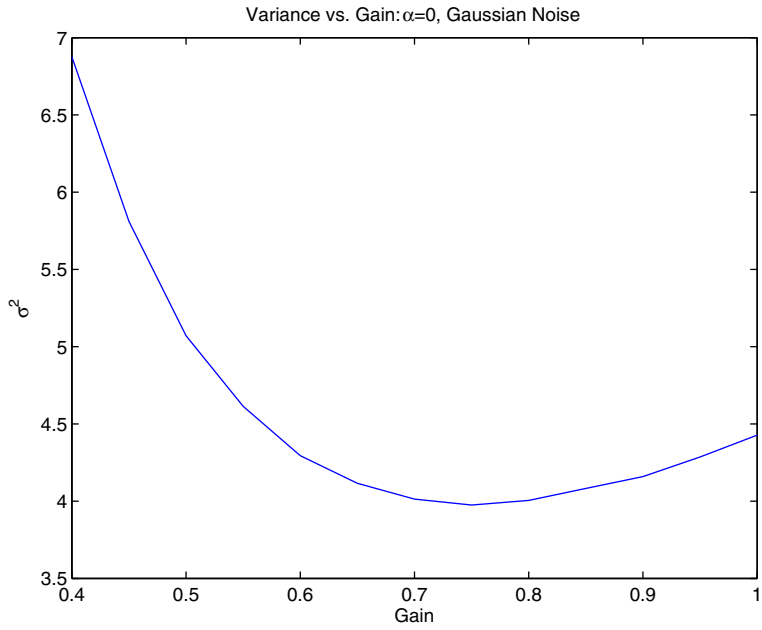

Fig. 33 Variance vs. gain: integer controller with Gaussian noise

3. Then, this same simulation was performed with non-Gaussian noise, under which the system produced nearly the same results, however with the ARD, the variance was not as consistent over the range of gains as the Gaussian case.
4. Next, the fractional-order system was used, with Gaussian noise. The value of the integrator order, α was varied to find a minimum variance. The gain of the I^{α} term was set to the optimal value found in simulation 1, $k = 0.75$. This produced an optimal value of $\alpha = -0.18$.

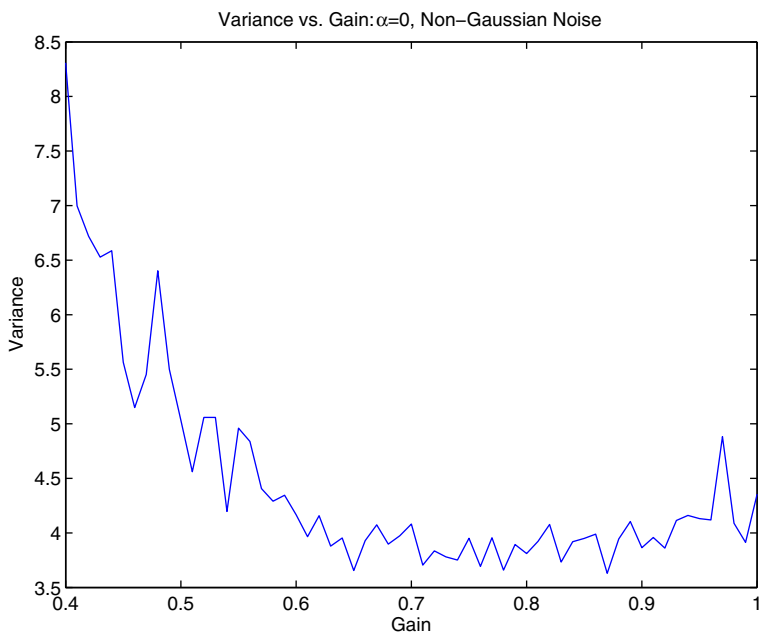

Fig. 34 Variance vs. gain: integer controller with non-Gaussian noise

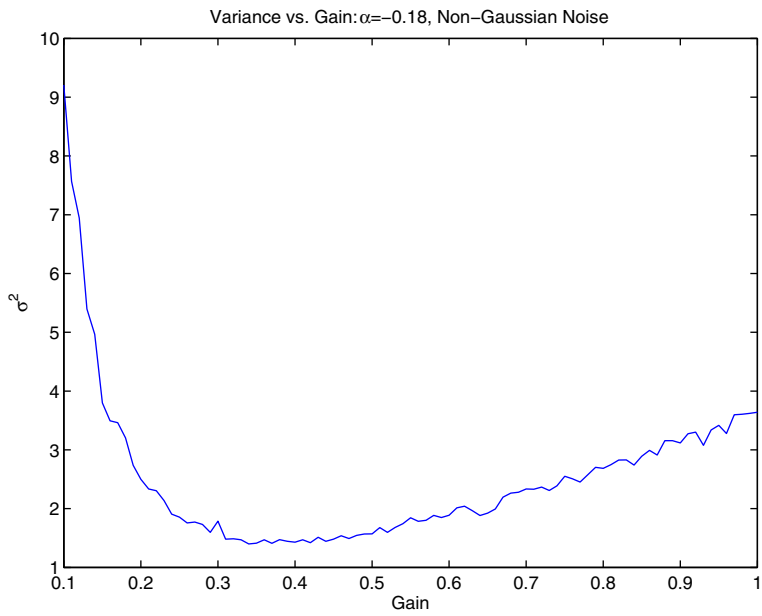

Fig. 35 Variance vs. gain: fractional-order controller with Non-Gaussian noise and $\alpha = -0.18$ found numerically

5. The fractional-order system was then tested with non-Gaussian noise, and shown to give the same $\alpha = -0.18$ minimum variance as with the Gaussian case.
6. Finally, using the optimum $\alpha = -0.18$ found above, the controller gain k was optimized for the fractional order controller and non-Gaussian noise case (Fig. 35). This gain, $k = 0.35$ is much lower than the integer-order case, while providing less than $\frac{1}{2}$ the variance, at $\sigma^2 = 1.52$.

From these simulations, it is clear that the fractional-order filter outperforms the integer-order filter. With a low-order integrator (less than 0.2), and comparatively low gain, the fractional-order controller nearly halves the variance of the integer-order controller.

5 Guidelines for Complementary Filter Use in Small UAS

Kalman or Kalman-style combining filters are the established solution for combining sensor data into navigation-ready data. Extended Kalman filter approaches allow non-linear models to be used and estimated with the Kalman techniques; however, these models are linearized and assumptions are made that the estimates do not deviate too far from the nominal solution. They have also proved difficult to apply to small UAS with low-cost, high-noise sensors [26, 44]. Complementary filters are not mathematically rigorous like the Kalman filter, and are therefore not well-suited for high-risk applications like space borne missions. However, compared to Kalman filtering, complementary filter techniques are less computationally intensive and more readily performed on small, low-power computing hardware, which is ideal for small, low-cost UASs.

Although Gaussian statistical models are traditional and have a wide range of applications, non-Gaussian, power-law statics are ubiquitous in practice [34]. Although augmented Kalman-style filters (such as the Kalman–Levy filter) that allow non-Gaussian PDFs have been considered in research, they are not well studied and have even higher mathematical complexity than standard Kalman techniques [20].

Complimentary filters work without assuming Gaussian noise statistics and are applicable to a wider variety of sensor hardware such as commonly-available MEMS devices with longer-tail noise tendencies [29]. Since complementary filters require less computational power, they

couple well with low-cost MEMs sensors and microcontrollers and can be better suited to the navigation needs of small, low-cost UASs.

Our suggested guidelines include (1) understand each sensor's pros and cons; (2) understand the tradeoff objectives; (3) whenever possible, as demonstrated in this paper, try to iteratively decide the best cut-off frequency; and (4) use as much domain knowledge as possible when deciding the design parameters linked to the complementary filter design.

6 Conclusion

Navigation is critical for UASs to fly safely and for collection of scientific mission data. In order to perform this task with lower cost and higher accuracy and reliability, better navigation data is critical, but must be weighed against the cost of the navigation systems if true low-cost personal remote sensing-level UASs are to be a reality. Other than the now standard Kalman filter, one way to fuse data from different sensors is to use a complementary filter. These complementary filters can be formulated in a traditional control system format, and can then be tuned like any control system. Fractional calculus is as old as the traditionally used calculus, but its use is still being investigated. When the concepts of fractional calculus are introduced into the complementary filter, it is shown that it is possible to achieve much better performance from noisy sensors, in this case, more than double the performance as evaluated by variance.

Future work includes noise modeling of physical navigation sensors, testing of fractional-order complementary filters on real flight data, and eventually implementation and flight with a real UAS.

Acknowledgements The authors would like to acknowledge Dr. Mac McKee of the Utah Water Research Laboratory. Thanks are owed to Dr. Gary Bohannan of the University of Saint Cloud, Minnesota, Dr. Igor Podlubny of the Technical University of Technical University of Košice, Slovak Republic, as well as the members of the fractional order calculus and UAS research community.

This work is supported by Utah Water Research Laboratory MLF 2006-2013.

References

1. Paparazzi: The Free Autopilot (an opensource project). http://paparazzi.enac.fr/. Accessed 4 Oct 2013
2. Anderson, W., Fritze, E.: Instrument approach system steering computer. Proc. Inst. Radio Eng. **41**(2), 219–228 (1953). doi:10.1109/JRPROC.1953.274209
3. Bachmann, E.R., Duman, I., Usta, U.Y., McGhee, R.B., Yun, X.P., Zyda, M.J.: Orientation tracking for humans and robots using inertial sensors. In: Proc. of the IEEE International Symposium on Computational Intelligence in Robotics and Automation, pp. 187–194 (1999). doi:10.1109/CIRA.1999.810047
4. Bachmann, E.R., McGhee, R.B., Yun, X., Zyda, M.J.: Inertial and magnetic posture tracking for inserting humans into networked virtual environments. In: Proc. of the ACM Symposium on Virtual Reality Software and Technology VRST, p. 9. ACM Press (2001). doi:10.1145/505008.505011
5. Bachmann, E.R., McKinney, D., McGhee, R.B., Zyda, M.J.: Design and implementation of MARG sensors for 3-DOF orientation measurement of rigid bodies. In: Proc. of the IEEE International Conference on Robotics and Automation, pp. 1171–1178 (2003). doi:10.1109/ROBOT.2003.1241751
6. Baerveldt, A.J., Klang, R.: A low-cost and low-weight attitude estimation system for an autonomous helicopter. In: Proc. of the IEEE International Conference on Intelligent Engineering Systems, pp. 391–395 (1997). doi:10.1109/INES.1997.632450
7. Baldwin, G., Mahony, R., Trumpf, J., Hamel, T., Cheviron, T.: Complementary filter design on the special euclidean group SE(3). In: Proc. of the European Control Conference, vol. 1, pp. 3763–3770 (2007)
8. Barton, J.D.: Fundamentals of small unmanned aircraft flight. Johns Hopkins APL Tech. Dig. **31**(2), 132–149 (2012)
9. Bohannan, G.: Analog realization of a fractional control element—revisited. In: Proc. of the 41st IEEE Int. Conf. on Decision and Control, Tutorial Workshop, vol. 1, pp. 27–30 (2002)
10. Brown, R.G., Hwang, P.Y.C.: Introduction to Random Signals and Applied Kalman Filtering, 2nd edn. No. 4 in Wiley, TK5102.5.B696. John Wiley & Sons (1997). doi:10.1521/ijgp.2010.60.4.455
11. Bryson, M., Sukkarieh, S.: Vehicle model aided inertial navigation for a UAV using low-cost sensors. In: Proc. of the Australasian Conference on Robotics and Automation (2006)
12. Butler, H., de Hoon, C.: Fractional-order filters for active damping in a lithographic tool. Control Eng. Pract. **21**(4), 413–419 (2013). doi:10.1016/j.conengprac.2012.12.011
13. Chao, H., Coopmans, C., Di, L., Chen, Y.: A comparative evaluation of low-cost IMUs for unmanned autonomous systems. In: Proc. of the 2010 IEEE Conference on Multisensor Fusion and Integration, pp. 211–216. IEEE (2010). doi:10.1109/MFI.2010.5604460
14. Chen, Y., Moore, K.L.: Discretization schemes for fractional order differentiators and integrators. IEEE

Trans. Circuits Syst. I: Fund. Theory Appl. **49**(3), 363–367 (2002)
15. Chen, Y., Vinagre, B.M., Podlubny, I.: Continued fraction expansion approaches to discretizing fractional order derivatives—an expository review. Nonlinear Dyn. **38**(1–4), 155–170 (2004). doi:10.1007/s11071-004-3752-x
16. Coopmans, C., Di, L., Jensen, A., Dennis, A., Chen, Y.: Improved architecture designs for a low cost personal remote sensing platform: flight control and safety. In: Proc. of the ASME IDETC/CIE 2011, 1st Small Unmanned Aerial Vehicle Technologies and Applications (SUAVTA), 2011 ASME/IEEE International Conference on Mechatronic and Embedded Systems and Applications (MESA11) (2011)
17. Coopmans, C., Han, Y.: AggieAir: An integrated and effective small multi-UAV command, control and data collection architecture. In: Proc. of the ASME IDETC/CIE 2009, 1st Small Unmanned Aerial Vehicle Technologies and Applications (SUAVTA), 2009 ASME/IEEE International Conference on Mechatronic and Embedded Systems and Applications (MESA09). San Diego, CA, USA (2009)
18. Coopmans, C., Stark, B., Coffin, C.M.: A payload verification and management framework for small uav-based personal remote sensing systems. In: Proc. of the 2012 Int. Symposium on Resilient Control Systems (ISRCS2012), pp. 184–189. IEEE (2012). doi:10.1109/ISRCS.2012.6309316
19. Crassidis, J.L., Markley, L.F., Cheng, Y.: Survey of nonlinear attitude estimation methods. J. Guid. Control. Dyn. **30**(1), 12–28 (2007)
20. Gordon, N., Percival, J., Robinson, M.: The Kalman–Levy filter and heavy-tailed models for tracking maneuvering targets. In: Proc. of the International Conference on Information Fusion, pp. 1024–1031 (2003)
21. Gorenflo, R., Mainardi, F.: Fractional calculus and stable probability distributions. Arch. Mech. **50**(3), 1–10 (1998)
22. Hamel, T., Mahony, R.: Attitude estimation on SO[3] based on direct inertial measurements. In: Proc. of the IEEE International Conference on Robotics and Automation, pp. 2170–2175 (2006). doi:10.1109/ROBOT.2006.1642025
23. Higgins, W.: A comparison of complementary and Kalman filtering. IEEE Trans. Aerosp. Electron. Syst. AES **11**(3), 321–325 (1975)
24. Jensen, A., Neilson, B., McKee, M., Chen, Y.: Thermal remote sensing with an autonomous unmanned aerial remote sensing platform for surface stream temperatures. In: Proc. of the International Geoscience and Remote Sensing Symp. (IGARSS), pp. 5049–5052 (2012)
25. Jensen, A.M., Chen, Y., McKee, M., Hardy, T., Barfuss, S.L.: AggieAir—a low-cost autonomous multispectral remote sensing platform: new developments and applications. In: Geoscience and Remote Sensing Symposium, 2009 IEEE International, IGARSS 2009, vol. 4, pp. IV–995–IV–998 (2009). doi:10.1109/IGARSS.2009.5417547
26. Jun, M., Roumeliotis, S.I., Sukhatme, G.S.: State estimation of an autonomous helicopter using Kalman filtering. In: Proc. of the IEEE/RSJ International Conference on Intelligent Robots and Systems, vol. 3, pp. 1346–1353 (1999). doi:10.1109/IROS.1999.811667
27. Kingston, D.B., Beard, A.W.: Real-time attitude and position estimation for small UAVs using low-cost sensors. In: Proc. of the AIAA Unmanned Unlimited Technical Conference, Workshop and Exhibit, pp. 2004–6488 (2004)
28. Krishna, B.T.: Studies on fractional order differentiators and integrators: a survey. Signal Process. **91**, 386–426 (2011)
29. Krobka, N.I.: Differential methods of identifying gyro noise structure. Gyrosc. Navig. **2**(3), 126–137 (2011)
30. Mahony, R., Hamel, T., Pflimlin, J.M.: Complementary filter design on the special orthogonal group SO(3). In: Proc. of the IEEE Conference on Decision and Control and European Control Conference, pp. 1477–1484 (2005)
31. Mahony, R., Hamel, T., Pflimlin, J.M.: Nonlinear complementary filters on the special orthogonal group. IEEE Trans. Autom. Control **53**(5), 1203–1218 (2008). doi:10.1109/TAC.2008.923738
32. Mahony, R., Hamel, T., Trumpf, J., Lageman, C.: Nonlinear attitude observers on SO(3) for complementary and compatible measurements: a theoretical study. In: Proc. of the IEEE Conference on Decision and Control held jointly with the Chinese Control Conference, pp. 6407–6412 (2009). doi:10.1109/CDC.2009.5399821
33. Monje, C.A., Chen, Y., Vinagre, B., Xue, D., Feliu, V.: Fractional Order Systems and Control—Fundamentals and Applications (Advanced Industrial Control Series). Springer-Verlag (2010)
34. Newman, M.E.J.: Power laws, Pareto distributions and Zipfs law. Contemp. Phys. **46**(5), 323–351 (2005)
35. Nolan, J.P.: Stable Distributions—Models for Heavy Tailed Data. Birkhauser, Boston (2013)
36. Oldham, K.B., Spanier, J.: The Fractional Calculus, vol. 17. Dover (1974)
37. Oliveira, P., Kaminer, I., Pascoal, A.: Navigation System Design Using Time-varying Complementary Filters. IEEE Transactions on Aerospace and Electronic Systems **36**(4), 1099–1114 (2000)
38. Oustaloup, A., Levron, F., Mathieu, B., Nanot, F.M.: Frequency-band complex noninteger differenciator: characterization and systhesis. IEEE Trans. Control Syst. I: Fundam. Theory Appl. **47**(1), 25–39 (2000)
39. Pflimlin, J.M., Hamel, T., Souères, P.: Nonlinear Attitude and Gyroscope's Bias Estimation for a VTOL UAV. Int. J. Syst. Sci. **38**(3), 197–210 (2007). doi:10.1080/00207720601110798
40. Plummer, A.R.: Optimal complementary filters and their application in motion measurement. Proc. Inst. Mech. Eng. Part I: J. Syst. Control Eng. **220**(6), 489–507 (2010)
41. Podlubny, I.: Fractional Differential Equations. Academic Press, San Diego (1999)
42. Podlubny, I., Petráš, I., O'Leary, P., Dorčák, L., Vinagre, B.M.: Analogue Realizations of Fractional Order Controllers, vol. 29 (2002)

43. Rehbinder, H., Hu, X.: Drift-free attitude estimation for accelerated rigid bodies. Automatica **40**(4), 653–659 (2004). doi:10.1016/j.automatica.2003.11.002
44. Roberts, J.M., Corke, P.I., Buskey, G.: Low-cost flight control system for a small autonomous helicopter. In: Proc. of the IEEE International Conference on Robotics and Automation, vol. 1, pp. 546–551. Australian Robotics Automation Association (2002). doi:10.1109/ROBOT.2003.1241651
45. Salcudean, S.: A Globally convergent angular velocity observer for rigid body motion. IEEE Trans. Autom. Control **36**(12), 1493–1497 (1991). doi:10.1109/9.106169
46. Shaw, F.R., Srinivasan, K.: Bandwidth enhancement of position measurements using measured acceleration. Mech. Syst. Signal Process. **4**(1), 23–38 (1990). doi:10.1016/0888-3270(90)90038-M
47. Sheng, H., Chao, H., Coopmans, C., Chen, Y., Mckee, M.: Low-cost UAV-based thermal infrared remote sensing: platform, calibration and applications. In: Proc. of the 2010 IEEE/ASME International Conference on Mechatronic and Embedded Systems and Applications, pp. 38–43. Qingdao, ShanDong, China (2010). doi:10.1109/MESA.2010.5552031
48. Sheng, H., Chen, Y., Qiu, T.: Fractional Processes and Fractional-Order Signal Processing: Techniques and Applications. Springer (2012)
49. Shiau, J.K., Huang, C.X., Chang, M.Y.: Noise Characteristics of MEMS Gyro's Null Drift and Temperature Compensation. Appl. Sci. Eng. **15**(3), 239–246 (2012)
50. Valério, D.: Ninteger (2008). http://www.mathworks.com/matlabcentral/fileexchange/8312-ninteger. Accessed 4 Oct 2013
51. Veillette, M.: STBL: Alpha Stable Distributions for MATLAB (2012)
52. Wirkler, W.H.: Aircraft Course Stabilizing Means (1951)
53. Zimmermann, M., Sulzer, W.: High bandwidth orientation measurement and control based on complementary filtering. In: Proc. of the SYROCO IFAC Symposium on Robot Control. Vienna, Austria (1991)